

POLAR ALIGNMENT OF A PROTOPLANETARY DISK AROUND AN ECCENTRIC BINARY

REBECCA G. MARTIN¹ AND STEPHEN H. LUBOW²¹Department of Physics and Astronomy, University of Nevada, Las Vegas, Las Vegas, NV 89154, USA²Space Telescope Science Institute, Baltimore, MD 21218, USA*Draft version February 3, 2017*

ABSTRACT

We use three-dimensional hydrodynamical simulations to show that an initially mildly misaligned circumbinary accretion disk around an eccentric binary can evolve to an orientation that is perpendicular to the orbital plane of the binary (polar alignment). As the disk evolves to the perpendicular state, it undergoes nodal libration oscillations of the tilt angle and the longitude of the ascending node. Dissipation within the disk causes the oscillations to damp. The process operates above a critical initial misalignment angle that depends upon the eccentricity of the binary and the mass of the disk. For binary eccentricity of 0.5, the process operates typically for disk masses smaller than a few percent of the binary mass and initial tilt angle of more than 40 degrees. This evolution has important implications for planet formation around eccentric binary star systems.

Subject headings: accretion, accretion disks – binaries: general – hydrodynamics – planets and satellites: formation

1. INTRODUCTION

Most stars form in binary or multiple systems (Ghez et al. 1993; Duchêne & Kraus 2013) and circumbinary and circumbinary disks likely form in these systems (e.g. Dutrey et al. 1994). Stars form in molecular clouds which are turbulent (e.g. McKee & Ostriker 2007). This environment may lead to chaotic accretion during the star formation process (Bate et al. 2003). The result is that circumbinary disks may form misaligned to the orbital plane of the binary (Monin et al. 2007; Bate et al. 2010). Planet formation likely occurs in these disks and so understanding the evolution of disks in these systems is vital for explaining exoplanet properties.

Misalignments have been observed at different evolutionary stages of binary star systems. The pre-main sequence binary KH 15D has a circumbinary disk that is inclined and precessing with respect to the binary orbital plane (e.g. Winn et al. 2004; Chiang & Murray-Clay 2004; Capelo et al. 2012). The circumbinary disk around the binary protostar IRS 43 has a misalignment of at least 60° (Brinch et al. 2016). Main-sequence stars in binaries with separations greater than about 40 AU have spin rotation axes that are misaligned to their binary orbital rotation axes (Hale 1994). Misaligned disks around each component of binaries are common (e.g. Stapelfeldt et al. 1998; Jensen & Akeson 2014; Williams et al. 2014). Binary 99 Herculis has orbital eccentricity 0.76 and a misaligned debris disk. The most likely inclination for the disk is perpendicular to the binary orbital plane (Kennedy et al. 2012). Finally, exoplanets are observed with orbits tilted with respect to the spin axis of the central star (Albrecht et al. 2012; Winn & Fabrycky 2014).

For a small level of misalignment with respect to the binary orbital plane of a circular orbit binary, nearly circular circumbinary test particle orbits undergo gyroscopic motion about the orbital rotation axis of the binary. In this case, particle orbits exhibit nodal precession that is fully circulating with nearly constant tilt. But for larger

tilts involving eccentric binaries, the situation is more complicated. Test particle orbits around a misaligned eccentric binary sometimes undergo nodal libration (rather than circulation), together with inclination oscillations (Farago & Laskar 2010; Doolin & Blundell 2011). The critical misalignment angle above which this mechanism operates decreases with the eccentricity of the binary. For circular orbit binaries, the mechanism does not operate. For low eccentricity, $e = 0.2$, the critical inclination is about 60° while for higher eccentricity, $e = 0.5$, the critical angle is about 40°.

A slightly misaligned circumbinary disk has been predicted to align with the binary orbital plane through viscous dissipation (e.g. Nixon et al. 2011; Foucart & Lai 2013, 2014). The dynamics of misaligned circumbinary disks have previously been studied, but the studies typically assumed that either the binary orbit is circular (e.g. Nixon 2012; Facchini et al. 2013; Lodato & Facchini 2013; Foucart & Lai 2013) or that the binary orbit is eccentric but coplanar to the disk (e.g. Artymowicz & Lubow 1994; Dunhill et al. 2015; Fleming & Quinn 2016). Aly et al. (2015) examined the misaligned and eccentric case for cold black hole disks. They observed precession about the eccentricity vector of the binary (rather than the orbital rotation axis of the binary), with a cold disk, and aspect ratio less than the viscosity parameter, $H/R < \alpha$. The disk tore into disjoint radial regions leading to violent interactions (see also Nixon et al. 2013). In this work we focus on the wave-like regime in which $H/R > \alpha$ relevant to protoplanetary disks.

In Section 2 we first reexamine test particle orbits around a misaligned eccentric binary for parameters relevant to circumbinary disks around young stars. In Section 3 we then consider the evolution of a hydrodynamic protoplanetary disk around a misaligned and eccentric binary. In Section 4 we discuss the implications of our results and we draw our conclusions in Section 5.

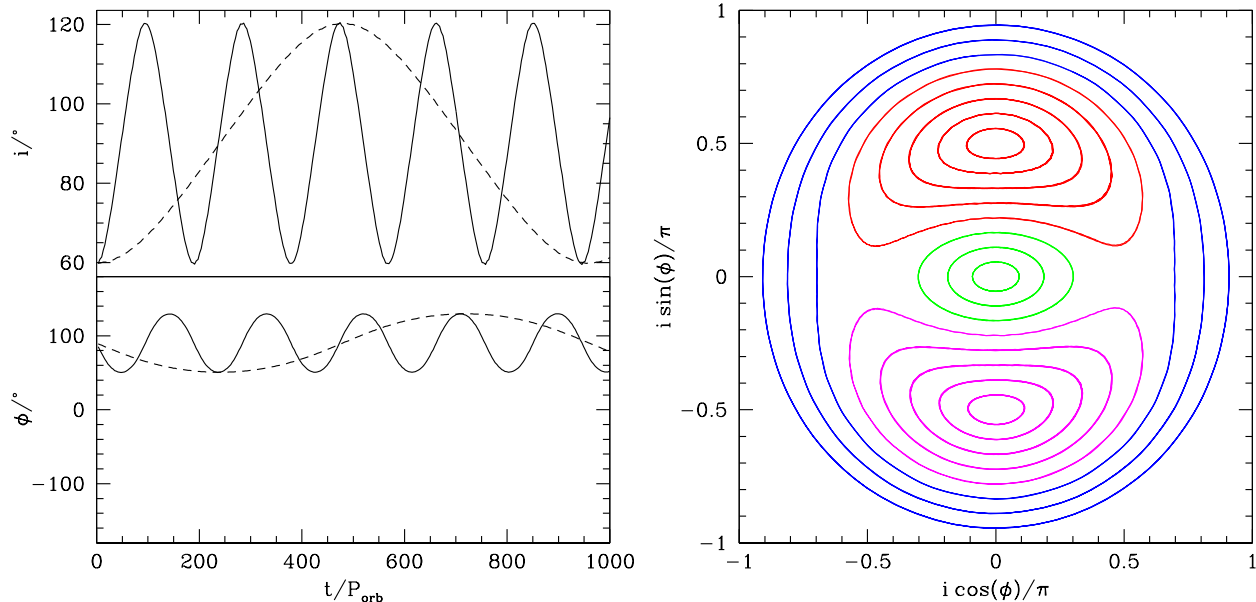


FIG. 1.— Initially circular test particle orbits around an eccentric binary with $e = 0.5$. Left: Time evolution of the inclination (upper panel) and the longitude of the ascending node (lower panel) for orbits initially inclined by $i_0 = 60^\circ$ to the binary orbit. The initial separation is $d = 5a$ (solid lines) and $d = 8a$ (dashed lines). The initial longitude of the ascending node is $\phi_0 = 90^\circ$. Right: The $i \cos \phi - i \sin \phi$ plane for orbits with varying initial inclination and longitude of the ascending node. The green lines show orbits close to prograde with $i_0 = 10^\circ$, $i_0 = 20^\circ$ and $i_0 = 30^\circ$ with $\phi_0 = 90^\circ$ in order of increasing size. The blue lines show orbits close to retrograde with $i_0 = 150^\circ$, $i_0 = 160^\circ$ and $i_0 = 170^\circ$ with $\phi_0 = 90^\circ$ in order of increasing size. The red lines show librating solutions with $i_0 = 80^\circ$, $i_0 = 70^\circ$, $i_0 = 60^\circ$, $i_0 = 50^\circ$ and $i_0 = 40^\circ$ with $\phi_0 = 90^\circ$ in order of increasing size. The magenta lines show librating solutions with $i_0 = 80^\circ$, $i_0 = 70^\circ$, $i_0 = 60^\circ$, $i_0 = 50^\circ$ and $i_0 = 40^\circ$ with $\phi_0 = -90^\circ$ in order of increasing size.

2. INCLINED CIRCUMBINARY TEST PARTICLE ORBITS

In this Section we consider inclined test particle orbits around an eccentric binary. The stars have equal mass $M_1 = M_2 = 0.5M$, where M is the total mass of the binary and they orbit with semi-major axis, a . The eccentricity of the binary is $e = 0.5$ and the orbital period is $P_{\text{orb}} = 2\pi/\sqrt{G(M_1 + M_2)/a^3}$. We work in the frame of the centre of mass of the binary. In Cartesian coordinates, with the binary orbit in the $x-y$ plane, the binary begins at periastron separation on the x axis.

The test particle begins in a circular Keplerian orbit at position $(0, d, 0)$ with velocity $(-\Omega_p \cos i_0, 0, \Omega_p \sin i_0)$, where $\Omega_p = \sqrt{G(M_1 + M_2)/d^3}$ is the Keplerian angular velocity about the centre of mass of the binary and i_0 is the initial particle tilt with respect to the binary orbital plane. The longitude of the ascending node is measured from the x -axis. These initial conditions correspond to an initial longitude of the ascending node of $\phi_0 = 90^\circ$.

The left panel of Fig. 1 shows the test particle orbit evolution for an initial inclination of $i_0 = 60^\circ$ for two different initial separations, $d = 5a$ and $d = 8a$. The upper panel shows the inclination of the orbit, i , and the lower panel shows the longitude of the ascending node, ϕ . The semi-major axis of the particle remains close to constant over the orbit. The inclination and the longitude of the ascending node show synchronous oscillations. The magnitude of the oscillations does not depend upon the distance of the particle from the centre of mass of the binary. However, the timescale for the oscillations increases with distance.

The right hand panel of Fig. 1 shows test particle orbits in the $i \cos \phi - i \sin \phi$ phase space. The test particles all begin at a separation of $d = 5a$, although the separation

does not affect the motion in this phase portrait, only the time taken to make a complete orbit. Above a certain initial inclination, the particle orbits undergo libration rather than circulation. The centre of the upper librating region corresponds to $i = 90^\circ$ and $\phi = 90^\circ$, while the centre of the lower librating region corresponds to $i = 90^\circ$ and $\phi = -90^\circ$. For higher binary eccentricity, the critical inclination tilt angle that separates the librating from circulating cases is smaller (see Doolin & Blundell 2011, for more details). When the third body is massive, the nodal libration region shrinks (see Fig. 5 in Farago & Laskar 2010). For a body with a mass of the order of a few percent of the binary mass, the region may be reduced somewhat for the configuration of bodies considered here. In the next Section we consider the evolution of a misaligned low mass circumbinary disk around an eccentric binary.

3. CIRCUMBINARY DISK SIMULATIONS

With hydrodynamic disk simulations we now analyze the evolution of a misaligned circumbinary disk around an eccentric equal mass binary. We use the smoothed particle hydrodynamics (SPH; e.g. Price 2012) code PHANTOM (Price & Federrath 2010; Lodato & Price 2010). PHANTOM has been used to model misaligned accretion disks in binary systems previously (e.g. Nixon 2012; Nixon et al. 2013; Martin et al. 2014; Fu et al. 2015) Table 1 contains a summary of the binary and disk parameters. The binary has equal mass components with total mass $M = M_1 + M_2$, and an eccentric orbit in the $x-y$ plane with semi-major axis, a . The accretion radius for particle removal from the simulation about each star is $0.25a$.

The upper panels in Fig. 2 show the initially flat and

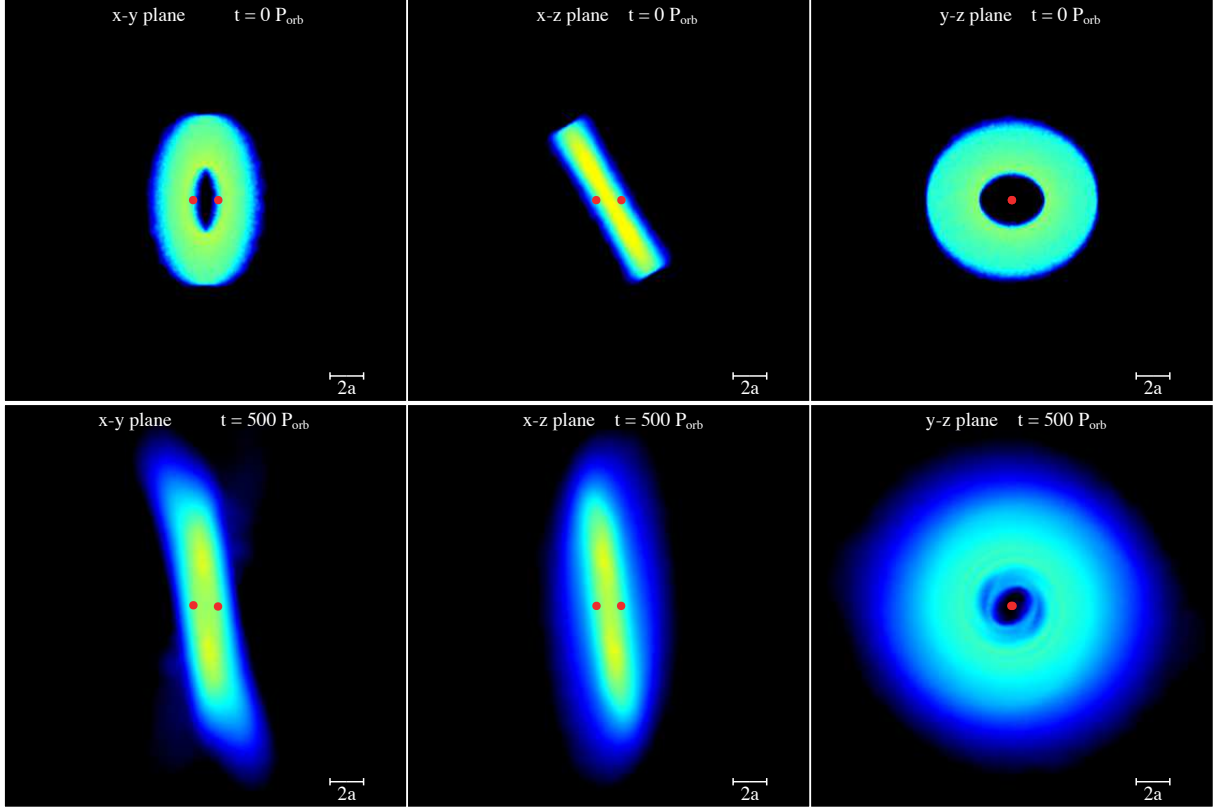


FIG. 2.— Upper panels: Initial disk set up for the SPH simulation of a binary (shown by the red circles) with an inclined circumbinary disk. Lower panels: The disk at a time of $t = 500 P_{\text{orb}}$. The color denotes the gas density with yellow regions being about two orders of magnitude larger than the blue. The left panels show the view looking down on to the binary orbital plane, the $x - y$ plane. The middle panels show the $x - z$ plane and the right panels show the $y - z$ plane. In the right hand panels the binary components lie in front of each other and so only one red point is seen.

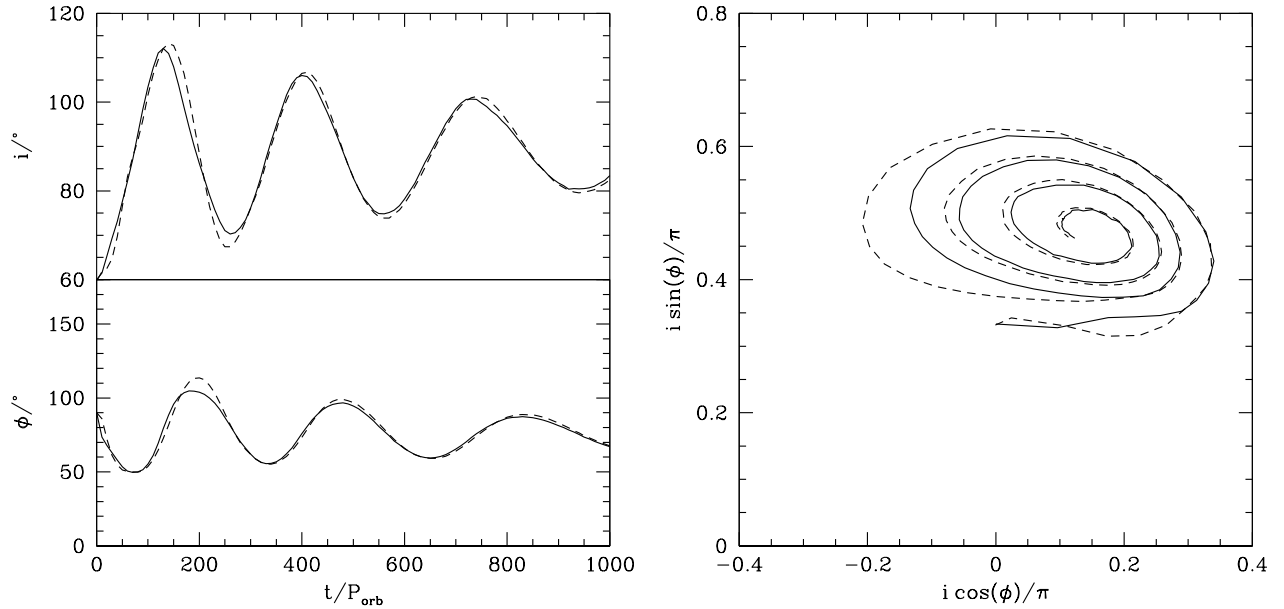


FIG. 3.— Left panel: Inclination (upper panel) and longitude of the ascending node (lower panel) for a circumbinary disk that is initially misaligned by $i_0 = 60^\circ$. The solid lines show the disk evolution at a radius of $3a$ and the dashed lines show a radius of $5a$. Right panel: The same simulation in the $i \cos \phi - i \sin \phi$ plane at a radius of $3a$ (solid line) and $5a$ (dashed line).

TABLE 1
PARAMETERS OF THE INITIAL CIRCUMBINARY DISK SET UP FOR AN
ECCENTRIC, EQUAL MASS BINARY WITH TOTAL MASS, M , AND
SEPARATION, a .

Binary and Disk Parameters	Symbol	Value
Mass of each binary component	$M_1/M = M_2/M$	0.5
Eccentricity of the binary	e	0.5
Accretion radius of the masses	R_{acc}/a	0.25
Initial disk mass	M_{di}/M	0.001
Initial disk inner radius	R_{in}/a	2
Initial disk outer radius	R_{out}/a	5
Disk viscosity parameter	α	0.01
Disk aspect ratio	$H/R(R = R_{\text{in}})$	0.1
	$H/R(R = R_{\text{out}})$	0.08
Initial disk inclination	i	60°

circular disk that is tilted to the binary orbital plane by 60° . The disk has initial mass $10^{-3}M$ distributed in 300,000 equal mass particles. The small disk mass has a minor dynamical significance on the orbit of the binary. Disk self-gravity is ignored. The initial surface density profile has a power law distribution $\Sigma \propto R^{-3/2}$ between $R_{\text{in}} = 2a$ and $R_{\text{out}} = 5a$. The inner radius of the disk is chosen to be close to the radius where a disk is tidally truncated (Artymowicz & Lubow 1994). However, misaligned disks feel a weaker binary torque (e.g. Lubow et al. 2015; Nixon & Lubow 2015; Miranda & Lai 2015). The disk is locally isothermal with sound speed $c_s \propto R^{-3/4}$ and $H/R = 0.1$ at $R = R_{\text{in}}$. This choice allows both α and $\langle h \rangle/H$ to be constant over the radial extent of the disk (Lodato & Pringle 2007). The Shakura & Sunyaev (1973) α parameter is taken to be 0.01 (the disk viscosity is implemented in the usual manner by adapting the SPH artificial viscosity according to Lodato & Price (2010) with $\alpha_{\text{AV}} = 0.4$ and $\beta_{\text{AV}} = 2.0$). The disk is resolved with shell-averaged smoothing length per scale height $\langle h \rangle/H \approx 0.25$.

In the left hand panel of Fig. 3 we show the time evolution of the inclination and the longitude of the ascending node of the disk at two orbital radii, $d = 3a$ and $d = 5a$. We clearly see damped nodal libration of the disk. As the inclination increases, the longitude of the ascending node decreases and vice versa. The evolution is very similar for different radii in the disk since the disk radial communication timescale is short enough for the nodal libration to occur globally. Dissipation causes the disk to move towards an inclination perpendicular to the binary orbit. The right hand panel shows the spiral in the $i \cos \phi - i \sin \phi$ plane as the disk tilt evolves towards being perpendicular to the binary orbital plane at the center of the librating region. We note that the spiral is slightly offset to the right of the diagram compared with the test particle orbits. This offset is due to the apsidal precession of the binary during the simulation due to the nonzero disk mass. This does not occur in the test particle case because the binary is not affected by the particle. The disk moves towards polar alignment perpendicular to the eccentricity vector of the binary. In the lower panels of Fig. 2, we show the disk at a time of $t = 500 P_b$ when the disk is almost perpendicular to the binary orbital plane.

4. DISCUSSION

Although we do not present the results here, we have also examined some different parameters for simulations. First, we have considered disks with a larger radial extent. We find for a disk initially outer truncated at larger radius that the evolution is at least initially qualitatively the same. The disk displays oscillations and moves towards a perpendicular orientation. The oscillations are more strongly damped for a disk with a larger radial extent. However, for disks truncated at radius $\gtrsim 10a$, there is some damping of the binary eccentricity. Lower binary eccentricity reduces the tendency for polar alignment. There is thus a competition between the timescales for the binary eccentricity damping and the polar alignment. Furthermore, if the alignment timescale becomes shorter than the sound crossing timescale, then disk warping will occur.

We have run the same simulation that is presented here, but with a circular binary and find that the alignment proceeds towards the binary orbital plane. We have also explored the evolution of a disk that begins close to counter alignment and find that the disk moves closer to counter-alignment. We have also considered the effect of a larger disk mass. We find that the accretion of material from a disk of mass $0.05M$ can circularise the binary. Furthermore, for large disk masses, the apsidal precession timescale of the binary may become shorter than the libration timescale of the disk, in which case the disk more closely follows a circulating solution. Both of these effects, accretion and precession, can result in disk–binary planar alignment, rather than polar alignment. If we observe a disk, or a planet, to be in a polar orbit, the eccentricity of the binary places constraints on the mass of the circumbinary disk. These effects will all be investigated in future work.

The circumbinary disk around the binary in KH 15D may be subject to the nodal and tilt oscillations described here. The binary eccentricity is high, $0.68 < e < 0.8$ (Johnson et al. 2004). For an eccentricity of 0.8, the mechanism described in this work would polar align the disk for a modest initial inclination of 20° and a low disk mass (see Doolin & Blundell 2011). A narrow ring disk has been invoked to explain the peculiar light curve. Thus the disk may be precessing about the eccentricity vector of the binary rather than the binary orbital axis. Over time, the disk will align with the polar axis rather than the binary orbital axis.

Kennedy et al. (2012) pointed out that the debris disk observed in 99 Herculis could be polar due to the stability of perpendicular particle orbits in this highly eccentric binary. In this model, the particles represent the solid debris. The results of this work suggest that the debris disk observed in 99 Herculis most likely arose from the evolution of a misaligned protostellar disk surrounding an eccentric binary. Because the eccentricity of the binary is very high at 0.76, the initial misalignment would not have to be very large. Material misaligned by only 20° to the binary orbital plane would evolve to become perpendicular. Thus, in binaries with large eccentricities, perpendicular disks may be more likely than coplanar disks. Debris disks and any planets that form in the disk may be more likely to be polar with orbital axes parallel to the binary eccentricity vector rather than aligned with the binary.

5. CONCLUSIONS

We have found that a polar alignment mechanism can operate for inclined disks around an eccentric binary star system. The mechanism operates best for higher binary eccentricity, larger initial disk misalignment angle, and lower disk mass. The inclination of the disk is exchanged with the longitude of the ascending node. Dissipation within the disk aligns the disk to be perpendicular to the binary orbital plane with disk rotation axis parallel to the binary eccentricity vector. The results have

many implications for circumbinary gas disks, circumbinary planets, and circumbinary debris disks.

S.H.L. acknowledges support from NASA grant NNX11AK61G. Computing resources supporting this work were provided by the UNLV National Supercomputing Institute. We thank Daniel Price for providing the PHANTOM code for SPH simulations and the SPLASH code (Price 2007) for data analysis and rendering of figures.

REFERENCES

- Albrecht, S., Winn, J. N., Johnson, J. A., Howard, A. W., Marcy, G. W., Butler, R. P., Arriagada, P., Crane, J. D., & et al. 2012, *ApJ*, 757, 18
- Aly, H., Dehnen, W., Nixon, C., & King, A. 2015, *MNRAS*, 449, 65
- Artymowicz, P. & Lubow, S. H. 1994, *ApJ*, 421, 651
- Bate, M. R., Bonnell, I. A., & Bromm, V. 2003, *MNRAS*, 339, 577
- Bate, M. R., Lodato, G., & Pringle, J. E. 2010, *MNRAS*, 401, 1505
- Brinch, C., Jørgensen, J. K., Hogerheijde, M. R., Nelson, R. P., & Gressel, O. 2016, *ApJ*, 830, L16
- Capelo, H. L., Herbst, W., Leggett, S. K., Hamilton, C. M., & Johnson, J. A. 2012, *ApJ*, 757, L18
- Chiang, E. I. & Murray-Clay, R. A. 2004, *ApJ*, 607, 913
- Doolin, S. & Blundell, K. M. 2011, *MNRAS*, 418, 2656
- Duchêne, G. & Kraus, A. 2013, *ARA&A*, 51, 269
- Dunhill, A. C., Cuadra, J., & Dougados, C. 2015, *MNRAS*, 448, 3545
- Dutrey, A., Guilloteau, S., & Simon, M. 1994, *A&A*, 286, 149
- Facchini, S., Lodato, G., & Price, D. J. 2013, *MNRAS*, 433, 2142
- Farago, F. & Laskar, J. 2010, *MNRAS*, 401, 1189
- Fleming, D. P. & Quinn, T. R. 2016, *ArXiv e-prints*
- Foucart, F. & Lai, D. 2013, *ApJ*, 764, 106
- . 2014, *MNRAS*, 445, 1731
- Fu, W., Lubow, S. H., & Martin, R. G. 2015, *ApJ*, 807, 75
- Ghez, A. M., Neugebauer, G., & Matthews, K. 1993, *AJ*, 106, 2005
- Hale, A. 1994, *AJ*, 107, 306
- Jensen, E. L. N. & Akeson, R. 2014, *Nature*, 511, 567
- Johnson, J. A., Marcy, G. W., Hamilton, C. M., Herbst, W., & Johns-Krull, C. M. 2004, *AJ*, 128, 1265
- Kennedy, G. M., Wyatt, M. C., Sibthorpe, B., Duchêne, G., Kalas, P., Matthews, B. C., Greaves, J. S., Su, K. Y. L., & Fitzgerald, M. P. 2012, *MNRAS*, 421, 2264
- Lodato, G. & Facchini, S. 2013, *MNRAS*, 433, 2157
- Lodato, G. & Price, D. J. 2010, *MNRAS*, 405, 1212
- Lodato, G. & Pringle, J. E. 2007, *MNRAS*, 381, 1287
- Lubow, S. H., Martin, R. G., & Nixon, C. 2015, *ApJ*, 800, 96
- Martin, R. G., Nixon, C., Lubow, S. H., Armitage, P. J., Price, D. J., Doğan, S., & King, A. 2014, *ApJL*, 792, L33
- McKee, C. F. & Ostriker, E. C. 2007, *ARA&A*, 45, 565
- Miranda, R. & Lai, D. 2015, *MNRAS*, 452, 2396
- Monin, J.-L., Clarke, C. J., Prato, L., & McCabe, C. 2007, *Protostars and Planets V*, 395
- Nixon, C., King, A., & Price, D. 2013, *MNRAS*, 434, 1946
- Nixon, C. & Lubow, S. H. 2015, *MNRAS*, 448, 3472
- Nixon, C. J. 2012, *MNRAS*, 423, 2597
- Nixon, C. J., King, A. R., & Pringle, J. E. 2011, *MNRAS*, 417, L66
- Price, D. J. 2007, *Pasa*, 24, 159
- . 2012, *Journal of Computational Physics*, 231, 759
- Price, D. J. & Federrath, C. 2010, *MNRAS*, 406, 1659
- Shakura, N. I. & Sunyaev, R. A. 1973, *A&A*, 24, 337
- Stapelfeldt, K. R., Krist, J. E., Ménard, F., Bouvier, J., Padgett, D. L., & Burrows, C. J. 1998, *ApJL*, 502, L65
- Williams, J. P., Mann, R. K., Di Francesco, J., Andrews, S. M., Hughes, A. M., Ricci, L., Bally, J., Johnstone, D., & Matthews, B. 2014, *ApJ*, 796, 120
- Winn, J. N. & Fabrycky, D. C. 2014, *ArXiv e-prints*
- Winn, J. N., Holman, M. J., Johnson, J. A., Stanek, K. Z., & Garnavich, P. M. 2004, *ApJ*, 603, L45